SOME OBSERVATIONS ON THE STRUCTURE AND MODELING OF 3-D TURBULENT BOUNDARY LAYERS AND SEPARATED FLOW

Roger L. Simpson
Aerospace and Ocean Engineering Department
Virginia Polytechnic Institute and State University
Blacksburg, VA 24061, USA
simpson@aoe.vt.edu

ABSTRACT

This paper presents some key features of the behavior and structure of three-dimensional turbulent boundary layers and separated flows that have been observed through experiments. These include the anisotropic nature of the eddy viscosity and the lags between the mean flow gradients and the turbulent stresses. These cases are rarely in equilibrium so lags between the production, diffusion, redistribution, and dissipation mechanisms become important. The skewing of the mean flow leads to decorrelation of the turbulent structure. Large-scale meandering vortical motions are often present in separated flows. Some computations of these types of flow are also examined. Better modeling of pressure and turbulence diffusion and pressure/rate-of-strain terms to account for lags within the flow is needed, especially near the wall. Some advances in experimental techniques that promise to provide more insights to such flows are mentioned.

INTRODUCTION

Three-dimensional turbulent boundary layers (3DTBL) occur in many practical cases, which are mostly non-equilibrium flows. The imposed wall pressure gradient or wall acceleration span-wise to the approach viscous flow creates a stream-wise vorticity flux at the wall and causes a change in direction of the flow as a function of distance from the wall. The purpose of this article is to give some features of the structure of such flows as revealed from experiments and to examine some recent modeling efforts.

Simpson (1996, 2001) and Simpson et al. (1997) presented perspectives on the behavior of incompressible 3DTBL and wing/body junction type flows and reviewed many related referenced works, which are not cited here. Here we will summarize first the key insights and conclusions from those works and augment them with some observations from recent work. A principal example geometry is the 3-D turbulent boundary layer and horseshoe junction flow (approach momentum thickness Reynolds numbers of $500 < Re_\theta < 23000$) around a 3:2 elliptic nose, NACA 0020 tail wing (Figure 1). Some results on the coherent turbulent structure, surface pressure fluctuations, and surface roughness effects are discussed. Other example flows are initially 2-D flows in curved ducts, over a swept bump or an axisymmetric bump, and flows over bodies of revolution at angles of attack. Modeling and calculations for these cases are discussed. While the reference list here is incomplete due to space limitations, much other work can be traced through these cited articles. Finally, some comments will be made on needed future work.

EARLIER INSIGHTS WITH NEW FEATURES

Simpson (1996) and Johnston and Flack (1996) implicitly show that many recently revealed features of 3DTBLs are due to the use of three-velocity-component laser-Doppler anemometry. In the Virginia Tech work, specially-designed fine-spatial-resolution (30μm spherical measurement volume diameter) fiber-optic laser-Doppler velocimeters (LDV) are used for point-wise and two-point spatial correlation measurements as close to the wall as $y^+ = yU_\tau/\nu = 3$ (Ölçmen and Simpson, 1995b; Byun et al., 2004). Although one should be able to infer a low uncertainty wall shearing stress $\tau_w = \rho U_\tau^2$ from the nearest-wall LDV velocity profile, Johnston and Flack suggest that there is a continuing need for improved direct measurement of τ_w.

For a mean 3-D turbulent boundary layer, the Reynolds-averaged flow structure at a given x,z location has an upstream history from a wedge-shaped "zone of dependence". The near-wall flow has a history from one direction and the near free-stream flow has a history from a different direction (Figure 2). As discussed below, the coherency between the inner and outer region turbulent motions from these different directions is less than for a 2-D case. Consequently, it is unlikely that similarity variables can be found to scale a strongly non-equilibrium 3-D flow. Special cases in which the 3-D mean flow only depends on 2 spatial variables x,y may have some similarity, since the mean flow at each x,y has the same history for all z (Simpson, 1996).

Examination of a number of data sets shows that no universal law-of-the-wall mean-velocity profile exists. If an overlap region exists between viscous wall region scales and large eddy outer region scales for moderate flow skewing, semi-logarithmic mean velocity and mean flow angle profiles exist in that region. Local near-wall equilibrium along some flows cause the mean velocity profiles to be self-similar in wall co-ordinates, but without a universal mean-velocity profile law. A law-of-the-wall semi-logarithmic mean velocity profile with universal constants only seems to exist for the beginning stages of a 3-D flow. Without a relationship with universal constants, the law-of-the-wall concept loses much of its usefulness.

For example, the mean velocity profiles deviate significantly from semi-logarithmic behavior for the complex lee-side 3DTBL on a swept bump (Webster et al.,1996), which grew rapidly, but did not separate. The discontinuities in wall curvature near the leading and trailing edges of the bump triggered internal layers. In agreement with previous investigations, the shear-stress vector

lagged the velocity-gradient vector despite the span-wise flow changing direction on the downstream side of the bump.

Experimental data show that the mean turbulent shearing stress direction is different from the mean flow direction and generally lags the local mean velocity gradient direction (Figure 3), so that the eddy viscosity (EV) is highly anisotropic in 3-D flows. An isotropic eddy viscosity turbulence model cannot reflect the correct physics of the stress-producing structures, although they continue to be widely used in calculations, largely because of their relative simplicity compared to other models. These models are weak approximations to the flow physics and are not robust for strongly 3-D cases, such as separated flows. Accelerating portions of 3D flows with weak cross-flows may be adequately calculated with this approach, but adverse pressure gradient flows are not well calculated in detail.

As confirmed again by the pressure-driven 3DTBL experiment of Compton and Eaton (1997), there is a reduction in the correlation between the shearing stress and the turbulent kinetic energy. This is due to the different histories of the outer layer and inner layer stress-producing flow structures - they come from different upstream directions (Figure 2). This reduction in shearing stress level requires significant skewing of the flow near the wall and may occur with asymmetric wall structures present without a mean 3-D flow, as pointed out by Eaton (1995) in his review. The observed reduction in eddy viscosity magnitude, as compared to algebraic eddy viscosity models, is due to decorrelation of turbulent structures and not due to non-equilibrium lags in a 2-D mean flow turbulence structure, which usually accompany strong adverse pressure gradients in 2D cases.

The eddy viscosity for the spanwise direction ν_z is not a constant factor N_e times the stream-wise eddy viscosity ν_x and depends upon the co-ordinate system. N_e appears to be about constant in the outer layer but varies much near the wall. Also the new vorticity comes from the wall and the outermost region behaves much like an inviscid rotational flow. Thus, in more detail than presented here, Simpson (1996) and Simpson et al. (1997) discuss the data and suggest that N_e = 0.6 in a wall-shearing-stress co-ordinate system or local streamline co-ordinate system can approximately account for anisotropy in eddy viscosity calculation methods in many flows. This prescription of co-ordinate system forces the span-wise shearing stress near the wall to approach zero either with a constant or varying N_e since the cross-flow velocity gradient $\partial W/\partial y$ is zero at the wall.

WING/BODY 3-D FLOWFIELD OVER A RANGE OF REYNOLDS NUMBERS

The well-documented wing/body junction low-speed flows (approach flow 500 < Re_θ < 23,000) of Ölçmen and Simpson (1995a, 1996a), Fleming and Simpson (1997), and Ölçmen and et al. (1999) can be used as computational test cases of turbulence models, as pointed out by Rizzi and Vos (1998). The mean 2-D upstream flow develops into a non-equilibrium 3-D flow and then relaxes back toward a mean 2-D flow far downstream. In addition to measurements along the path shown in Figure 1, which is outside the region near the wing where large mean flow stream-wise vortices are dominant, the mean flowfield and Reynolds stresses have been obtained over large regions of these geometry: (1) the nose separated flow and juncture vortex around the side of the wing, which is briefly discussed below (Ölçmen and Simpson, 1997b, Simpson, 2001); (2) the mean 2-D flow entrance conditions (Ölçmen and Simpson, 1995a); and (3) the downstream wake region. In addition, convective heat-transfer and the temperature field have been measured for this flowfield. See Simpson et al. (1997) for more references.

Upstream of the influence of the pressure gradients, which are produced by the presence of the wing, there is only span-wise mean vorticity in the approach flow. Span-wise pressure gradients introduce a flux of stream-wise vorticity and non-zero $\partial^2 W/\partial y^2$ at the wall, as given by

$$\frac{\partial^2 (W/U_\tau)}{\partial (y^+)^2} = \frac{1}{2}\frac{\partial (C_p)}{\partial (z/t)}\left(\frac{U_{ref}}{U_\tau}\right)^2\left(\frac{\nu}{tU_\tau}\right)$$

where t is the thickness of the wing and C_p is the pressure coefficient based on U_{ref}.

Figure 4 shows mean velocity profiles for approach Reynolds numbers Re_θ of 5940 and 23,200 at these stations in local wall shear stress coordinates and normalized on wall shear velocity U_τ and length ν/U_τ scales. The skin-friction values used in U_τ were obtained by fitting the viscous sublayer mean velocity profiles. As in other data sets, there is no universal law-of-the-wall profile. In the upstream flow direction or wind tunnel coordinates (Simpson, 1996), the streamwise wind tunnel mean flow velocity U first slightly decelerates due to the adverse pressure gradient and then accelerates around the wing.

The maximum W/U_τ magnitude in tunnel coordinates increases along the flow (Figure 5), is located progressively further from the wall, and varies similarly at both Reynolds numbers (5940 and 23,200) due to the similar distributions of the wall static pressure. Within experimental uncertainties, the left side of the above equation is about the same for the two cases for stations 1-6. For stations 7-9, the left side for the higher Re_θ case is about 2/3 of that for the lower Re_θ case. The pressure gradients are most effective on the low momentum lateral flow very near the wall and turn the flow progressively as the stream-wise vorticity is diffused toward the outer layer. The lateral pressure gradients are first positive and then negative. Thus, W decreases with large negative values until station 4 and then increases to form the wave-like velocity profiles at station 9. Because the $\partial^2(W/U_\tau)/\partial(y^+)^2$ wall boundary condition is about the same for the 2 Re_θ cases, at stations 1-6 the locations of the local peaks and minima in W/U_t profiles are also about the same. The W/U_τ near the wall begins to be different for stations 7-9. The outer layer $\partial W/\partial y$ at the higher Re_θ is practically zero at each station, indicating that stream-wise vorticity has not diffused completely through this much thicker layer at these stations. In the outer region, the turbulence acts as "frozen turbulence" that is convected by the flow. The Reynolds shearing stresses persist with the upstream 2DTBL magnitude and direction until the 3-D effects propagate to that location away from the wall. It appears that transport equations are needed to account for this nature of the lag within the flow. Even though Figure 5 shows some wall variables scaling, Eaton (1995) suggests that the span-wise velocity profile scales on the outer layer scales at various Reynolds numbers, although there are few 3DTBL studies over a significant range of Reynolds number.

Simpson et al. (1997) show a comparison of wind tunnel data (Re_θ = 5940) at Station 5 with the low Reynolds number (Re_θ = 500, 760, and 890) water tunnel data of Fleming and Simpson (1997) at the same station for flow around the same shaped wing. Both flowfields are subjected to almost the same non-dimensional pressure distributions around the wing. The U/U_e and W/U_e profiles in local free-stream direction co-ordinates scale fairly well in terms

of y/δ in the outer layer, apparently due to the turbulence-dominated transport and skewing of the vorticity in the outer layer. The largest Reynolds number effect is the increase in mean crossflow velocity with Reynolds number. The relative increase in viscous forces in the near-wall region at low Reynolds numbers tends to keep the boundary layer mean flow more closely aligned with the free-stream direction.

The turbulent kinetic energy (TKE = $q^2/2$), which is frequently used in turbulence modeling, also remains about frozen for stations 1 - 4. This suggests that the TKE is close to equilibrium with the production balanced by the sum of dissipation, net diffusion, and convection at each of these stations. As the flow accelerates at stations 5 - 7, the near-wall production of TKE causes a great increase of TKE for $10 < y^+ < 60$, while the TKE decreases slightly in the outer region.

The fluctuation terms are sensitive to Reynolds number for the lower Reynolds number range, $500 < Re_\theta < 5940$ (Simpson et al., 1997). While the u', v', and w' distributions have similar shapes over these Reynolds numbers, the profiles for a given stress cannot be scaled on either inner or outer variables to produce a collapse. This mainly reflects the Reynolds number dependence of the approach 2DTBL.

Like the magnitude of the shearing stress $|\tau/\rho|$, the TKE and the ratio of the two parameters ($|\tau/\rho|/2q^2 = a_1$), another parameter which is independent of rotation about the y axis is $|\tau/\rho|/v'^2 = 1/S$. For 2-D flows, S is near unity in the semi-log mean velocity profile region. For this 3-D flow, S is nearly a constant over an order of magnitude of y for a given profile. Ölçmen and Simpson (1995a) examined 9 other pressure-driven and shear-driven data sets and concluded that S is also about constant for a given profile for $y^+ > 50$ and $y/\delta < 0.6$, with values between 1 and 2. At stations where the 3-D effects are largest, S is higher than obtained for 2-D flows, which is due to less correlation between the u and v velocity fluctuation components. Fleming and Simpson (1997) show that the profiles of v'^2, -uv, and -vw, over the $500 < Re_\theta < 5940$ Reynolds number range do not correlate at the same stations in inner variables or outer variables, while 1/S collapses in inner variables.

There is no effect of Reynolds number on $1/S=|\tau/\rho|/v'^2$ vs. y^+ profiles near the wall throughout the flow for $890 < Re_\theta < 23200$. This indicates the strong relationship between the shearing stresses and the normal to the wall velocity fluctuations at all Reynolds numbers. This is in contrast to a_1, which varies much with 3-D effects and Reynolds number. On physical grounds, v' should be an important turbulence velocity scale, especially near the wall since the shear-stress-producing ejections and sweeps strongly determine v'. The a_1 parameter contains the u'^2 in the TKE, which reflects some of the inactive low frequency motions that do not contribute to the shear-stress producing motions. At the highest Reynolds number the skewness for the u and v fluctuations and the uw^2 correlation coefficient show an emerging semi-logarithmic variation in the middle of the boundary layer. This feature suggests an overlap between the inner and outer scales of motion that would expand for higher Reynolds numbers.

Using multiple probes in the wind tunnel flow, Ha and Simpson (1993) found that the coherency of larger-scaled structures is reduced by the effects of three-dimensionality. This length scale reduction occurs with the growth of 3-D turbulence effects near the wall that are unrelated to the outer region flow that originated from another direction in the upstream flow (Figure 2). Length scales in the outer region showed no change along the flow, indicating strong persistence of the coherency of outer region structures along the local free-stream direction. In the low Reynolds number cases, length scale results from auto-correlations revealed 50% shorter integral length scales for the 3-D flow as compared to a 2-D flow, which is consistent with the higher Reynolds number wind tunnel results.

The skewing angle of the coherent structures closely follows the local mean velocity angle especially in the inner region, indicating that the coherent structures are convected in the mean flow direction (Figure 3). In the outer layer at this location, equally coherent motions occur over a wider angular range between the far upstream 2-D flow direction and the local flow direction. This indicates that the direction of the far upstream outer region coherent motions lags for a long distance, even after being subjected to the skewing effects of local turbulence transport equation mechanisms.

Spatial correlations of v' (Ölçmen et al., 1998) in wall stress co-ordinates show that the downstream peak values are located further from the wall, while they are closer to the wall upstream. This variation suggests outgoing characteristics that are affected by only the upstream flow. The wallward sweeping ($u > 0$, $v < 0$) motions seem to have similarity near the wall. The correlations are skewed in the spanwise direction, with the peak correlation in the same direction as the sign of the $\overline{w^3}$. Ölçmen et al. (2005) show that using only the contributions from the sweep ($u > 0$, $v < 0$) and ejection ($u < 0$, $v > 0$) motions in joint probability functions for this 3-D flow leads to 7 algebraic relations among 7 of the triple products that fairly well represent the measured triple product data for the outer part of the flow.

Another phenomenon occurs for the wing/body junction flowfield shown in Figure 1 and is discussed in more detail by Simpson (2001). For a sufficiently blunt nose, such as this wing, the horseshoe vortex structure between the vortex and the flat wall shows aperiodic low-frequency chaotic switching between velocity states that produce double-peaked (bimodal) velocity histograms of the velocity component spanwise to the vortical core direction. This self-induced large-scale unsteadiness of wing/body junction nose separations is responsible for high surface pressure fluctuations and high heat transfer rates around the nose.

Clearly, it is inappropriate to combine the effects of these large-scale separation-induced chaotic vortices with the turbulence structure. A seemingly proper way to model the horseshoe vortex flow around the wing is to use a large-eddy simulation for the chaotic scales, which are more coherent, and a subgrid model for the less coherent turbulence that accompanies the boundary layer that approaches the wing.

Surface Pressure Fluctuations

Surface pressure fluctuation measurements were made in two-dimensional turbulent boundary layers at two Reynolds numbers (Re_θ = 7300, 23400) and at two approach Reynolds numbers (Re_θ = 5940, 23200) that form to the front and side of this wing/body junction (Goody and Simpson, 1999). Measurements were made at the stations in Figure 1. Spectral levels of surface pressure fluctuations measured in the 2-D flows are consistent with accepted behavior. The collapse of spectral levels scaled on local wall shear velocity U_τ and length ν/U_τ scales at middle and high frequencies was shown for a wide range of Reynolds number ($1400 < Re_\theta < 23400$). Also shown was the effect of Reynolds number on the size of an overlap frequency range in which both inner and outer boundary layer variables collapse the surface pressure spectra. Scaling parameters that collapse the pressure

spectra beneath 2-D flows do not collapse the pressure spectra beneath 3-D flows. The pressure spectra are nearly constant, or flat, within a mid-frequency range at some measurement stations in the 3-D flows. When compared to the 2-D flows, higher spectral levels within the flat and high frequency spectral ranges significantly raise p'. Additionally, dimensional spectral levels within the flat frequency range are independent of Reynolds number. An analysis based on the Poisson pressure fluctuation equation shows that the variation of the high frequency spectral levels are related to the variation in near-wall mean velocity gradients and $\overline{v^2}$ structure due to the span-wise mean pressure gradient. Thus, 3DTBLs can produce much larger p' levels than 2-D cases due to greater high frequency contributions from the near-wall behavior.

Some Effects of Surface Roughness

Wind tunnel experiments have been conducted for three-dimensional boundary layers developed over fetches of roughness elements upstream and around this wing-body junction at locations shown in Figure 1 (George and Simpson, 2002). For each fetch very uniform 0.078" diameter circular cylindrical roughness elements of either 0.015", 0.030", or 0.060" height were used in square and diagonal cell patterns, yielding six different cases of measurements. The $k^+ = kU_\tau/\nu$ values for these 3 heights in these flows are about 27, 61, and 140 with projected frontal area to projected wall area λ ratios of 0.025, 0.05, and 0.10, respectively. Figure 6 shows the downward shift of the streamwise mean velocity with increasing surface roughness. The data reveal that the surface pressure gradient distribution is not strongly influenced by the roughness elements, thus the local vorticity flux averaged over several cells is about the local smooth wall value. The effects of the span-wise pressure gradients imposed on the rough-wall boundary layers is seen in the significant mean flow skewing, close to the wall, within the elements and in the spanwise Reynolds shearing stresses, with peak levels comparable to those of the streamwise shearing stresses. The fact that W profiles, for both smooth as well as rough-wall layers, collapse in outer variables above 3 element heights (Figure 7) seems to indicate that the spatial average streamwise vorticity at each station is the same.The higher the roughness element height, the faster the diffusion of turbulence from wall to the outer layers. The effect of roughness pattern orientation is seen in the mean flow and turbulent structure only up to 3 roughness heights from the wall. The effect of three-dimensionality is also seen in the much higher transport of the turbulent kinetic energy by the fluctuations as compared to that by the fluctuations. George and Simpson (2005) show that the main production of TKE and Reynolds shearing stress occur just downstream of the element height. These data sets are test cases for comparisons with calculations.

Calculations for Wing-body Flow

Parneix et al. (1998) calculated this wing/body flow using the v^2-f model. This model uses the standard k - ϵ model, modified for near-wall turbulence anisotropy and non-local pressure-strain effects, and retains a linear eddy viscosity assumption. Calculations of the separation line are similar to the those revealed by the oil-flow visualizations and the wake results are fairly well represented. In the approach plane of symmetry the damping of the near-nose turbulent transport prevents the spurious production of turbulence near the wing that occurs with the k - ϵ model. Deng and Visonneau (1998) used a 2-equation scalar turbulence model and a near-wall second-moment closure to compute this flow. The Reynolds stress transport model simulated the anisotropic behavior of the normal Reynolds stresses and amplification of longitudinal vorticity. This anisotropy was also responsible for strong values of shearing stress $\overline{uw}$ near the horizontal surface. It seems clear that such improvements to Reynolds-averaged models are necessary in order to capture much of the important phenomena for complex vortical flows. Naturally since a Reynolds-averaged model cannot simulate the chaotic large-scale vortex structure in front of the nose, the high mean turbulent kinetic energy k around the mean vortex location is not well predicted. Large-eddy simulations (LES) should be used to capture the chaotic vortical motions.

FLOW OVER A 3-D BUMP

Byun and Simpson (2005) report fine-spatial-resolution three-velocity-component laser-Doppler velocimeter measurements for the separating 3DTBL over the leeside of an axisymmetric bump (Figure 8). Simpson et al. (2002), Byun et al. (2003), and Ma and Simpson (2005) present results for the downstream vortical wake. Mean velocities, Reynolds stresses and all triple products have been measured from the nearest bump surface. They show a saddle type 3-D separation at x/H $\approx$ 0.96 on the centerline of bump. The downstream backflow and the stream-wise flow from upstream of the saddle separation spread span-wise and generate one focus separation on each side at x/H $\approx$ 1.2 and z/H $\approx$ $\pm$0.7. The saddle-focus separated flow is not only on the nearest wall surface but also extends up to a normal to surface $y^+ \approx$ 340 based on the upstream U_τ. In the mean backflow region within $0° \le \psi \le 30°$, more TKE is generated than Reynolds shearing stresses. The large eddies and the flow from the bump side supply the mean backflow. Since the backflow region is intermittent in time, the large eddies supply the intermittently forward flow in this mean backflow region similar to a 2-D separated TBL. Bimodal probability distributions of U and W appear in this region due to the unsteady and low frequency meandering of the flow field. Significant symmetric bimodal histograms make the histogram edges smaller so that they occur with close to zero skewness and minimum flatness factors. Figure 8 illustrates flow features on the leeside of the bump.

Fureby et al.(2004) and Patel et al. (2003) used LES with an isotropic eddy viscosity model to be among the first to compute this flowfield. Compared with experiments, the Davidson and Dahlström (2005) hybrid LES-URANS calculations show only one counter clockwise rotating positive stream-wise vortex in a negative z/H side at a wake plane, even though the vortex center is closer toward the centerline than the measured vortex center. Their mean flow at the wall separates from about x/H $\approx$ 1 on the centerline, which is very close to the measured location. However, it has a weaker focus separation making a narrower spiral zone. On the other hand, the Wang et al. (2004) non-linear EV RANS results for skin friction lines agree better with the data than those of Davidson and Dahlström. However, the saddle separation occurs far upstream and there is a clockwise rotating negative streamwise vortex in a negative z/H side at wake planes in their models. The Temmerman et al. (2004) LES calculations for a 10 times lower Reynolds number flow show similar results as the Wang et al. results except much higher TKE level in the separated flow downstream than the RANS models. Also, their RANS and LES calculations show a much thicker mean backflow region downstream in the center plane up to x/H $\approx$ 3.5. Therefore, the entire flow structures over this bump need to be better modeled. Other calculations will be reported at the

11th ERCOFTAC/IAHR Workshop on Refined Turbulence Modelling (ERCOFTAC SIG 15), April 7-8, 2005, at Chalmers Univ., Göteborg, Sweden. The aim of this workshop is validation of (U)RANS and RANS-related (e.g., combined RANS/LES) models for flow and heat transfer.

As mentioned earlier, the LDV measurements show only one saddle and two foci mean separation points on the bump surface. It is expected that there is an attachment point on the centerline downstream. If this attachment point is nodal, as suggested by earlier oilflows (Simpson et al., 2002), then 2 saddle separation points must be present downstream in order to satisfy the surface kinematical rules. However, if there is a saddle reattachment point along the centerline, as suggested by the CFD calculations, then no additional separation points are needed to satisfy the kinematics. Therefore, to get complete flow features over this bump, measurements are needed for this reattachment and separation region downstream.

SWEPT SURFACE, DUCT AND CHANNEL FLOWS

Wu and Squires (1998)used large eddy simulation (LES) and Reynolds-averaged Navier–Stokes (RANS) computations to compute the swept bump flow of Webster et al. (1996). Subgrid-scale stresses in the LES were parameterized using the dynamic eddy viscosity model. Reynolds stresses in the RANS calculations were closed using the v^2-f model and Spalart–Allmaras one-equation model. The turning angle of the wall shear stress measured with respect to the upstream flow changes sign twice due to the alternating spanwise pressure gradient, with a maximum of more than 45 deg near the trailing edge. The mean flow is accurately predicted using both techniques, with some discrepancy occurring in prediction of the mean cross flow in the LES. Second-order statistics in the LES are in good agreement with measurements; RANS predictions of turbulence kinetic energy are slightly less accurate.

Paik et al. (2004) review recent progress using unsteady RANS (URANS) and detached eddy simulations (DES) for complex 3-D incompressible channel flows:(1) flow in a channel with four bottom-mounted rectangular piers; (2) flow in a channel with a corner-mounted rectangular block; and (3) flow in a strongly curved rectangular bend. Comparisons with experiments suggest that relatively simple turbulence closure models can simulate complex, 3D flows dominated by geometry induced, large-scale instabilities and unsteady coherent structures with reasonable accuracy. The results for the curved duct case show that an unsteady statistical turbulence model is necessary to compute the low-frequency, large-scale, vortical rolls in a concave wall boundary layer in order to simulate the dramatic effects of concave curvature on the structure of turbulence.

Bruns et al. (1999) describe an incompressible 3DTBL on the flat wall of an `S'-shaped wind tunnel test section under the influence of changing streamwise and spanwise pressure gradients produced by two opposite changes of core flow direction which causes a sign change of the spanwise pressure gradient accompanied by a reversal of the spanwise velocity component near the wall or the formation of so-called cross-over velocity profiles. Jongen et al. (1998) use an incompressible composite algebraic stress model that accounts for dissipation rate anisotropies, is calibrated against high-Reynolds number plane channel flow data, and is validated against a rectangular S-duct flow. The model calculated the mean velocity well, but not the shear stress magnitude and direction. The experimentally observed lag between the shear stress vector direction and the mean velocity-gradient vector direction is qualitatively predicted and the results are better than those from the tested isotropic eddy viscosity models.

After mentioning several recent works for U-bend flows, Suga (2003) presents calculations of turbulence and heat transfer in two types of square sectioned U-bend duct flows with mild and strong curvature by two recent second moment closures. The Batten et al. modified version of the Craft and Launder model was more reliable for strong curvature.

EXTERNAL FLOW OVER LIFTING BODIES - PROLATE SPHEROID AND SUBOFF SUBMARINE

The 6:1 prolate spheroid is a generic submarine-like body for which much previous mean flow data away from the wall and calculations have been obtained, as reviewed by Simpson (1996), but which lacked nearest-wall mean flow and turbulence data until the 3-velocity-component miniature fiber-optic LDV work by Chesnakas and Simpson(1997). The near-wall region is the most important region of a 3-D wall-bounded flow because most of the skewing of the velocity profiles occurs there. Measurements were made on the leeside in planes perpendicular to the model major axis for 10° and 20° angles of attack.

Figure 9 shows secondary flow patterns in planes of measurement. The initial stages and development of the open primary and secondary crossflow separations were defined and discussed in detail. From the LDV data and surface hot-film data, Wetzel et al. (1998) show that the local minima in skin friction magnitude coincide with the location of crossflow separation. Thus, Wetzel and Simpson (1998) were able to use this feature and hot-film data in obtaining the location of separations on this body during unsteady maneuvers.

These data support the 3-D turbulent flow observations discussed above. The ratio of the shearing stress magnitude to twice the TKE, A_1, takes on values near 0.1 at strongly skewed flow locations, which is much lower than the 0.15 value reported for mean 2-D flows. The ratio $1/S=|\tau/\rho|/v'^2$ shows values consistent with those for the Ölçmen and Simpson data. Madden and Simpson (1997)used the LDV data to examine the Reynolds stress contributions to each of the 8 octants of combinations of u, v, and w fluctuations in the local wall shearing stress co-ordinate system, which seems more closely aligned with the quasi-streamwise vortex structures than free-stream co-ordinates. Asymmetries that evolve between ejection ($u<0$, $v>0$) and sweep ($u>0$, $v<0$) motions with spanwise fluctuations (w) of opposite sign cause non-zero uw and vw in the buffer layer between the viscous sublayer and the semi-log region.

Goody et al. (1998)analyzed multiple hot-wire multi-velocity-component velocity spectral data obtained in the vortical separated flow of the prolate spheroid under the same flow conditions as examined by Chesnakas and Simpson. In regions with weaker 3-D effects, spectral features are similar to those for equilibrium flows. Spectra in strong vortical flow regions have unusual and apparently non-equilibrium features, which may be associated to some extent with the meandering of the vortices.

This behavior has some qualitative similarities with the surface pressure fluctuation spectra. Goody et al. (1997)show that the high frequency surface pressure fluctuations scale on wall variables. Near crossflow separation locations, p' is a local minimum, there is little high frequency content, and the dominant low frequencies are related to the outer layer flow. Around reattachments and under large vortices there are local maxima in p'.

Taylor et al. (2005), Sreenivas et al. (2005), and their cited earlier

works, show results over a SUBOFF submarine for 6 different RANS turbulence models that use the isotropic eddy viscosity assumption. The Wilcox stress-ω model produced the best comparisons with steady experimental force and moment coefficients for $-12^O < \alpha < 12^O$ angles of attack for a barebody. Rhee and Hino (2002)used a simple one equation model to simulate the unsteady maneuver of the prolate spheroid, which compared qualitatively well with the experiment of Wetzel and Simpson (1998).

Cummings et.al. (2003) discuss the importance of turbulence modeling and the difference between eddy-viscosity models and the stress-transport models. The eddy-viscosity models are based on the assumption that the Reynolds shear stresses are proportional to and aligned with the strain rate of the mean flow, which is not the case for crossflow separation. The stress-transport models make no such assumptions and should therefore be more correct in predicting the cross-flow separation on bluff bodies. Any attempt to use an eddy-viscosity model would result in tuning the model to conform to the particular case (6:1 prolate spheroid or SUBOFF). Morrison et al. (2003)reach the same conclusions with eddy viscosity vs. algebraic stress models.

In principle, because of the large-scale meandering motions of the vortical separated flow over these type bodies, one should use an URANS or LES to capture these measured features. Alin et al. (2005) and cited earlier works report both URANS and LES calculations for the prolate spheroid with several different isotropic subgrid models. Nevertheless, they report good agreement with the measured pressure coefficient and the correct location of separation.

Kottapati-Apparao et al. (2003) report Detached Eddy Simulations (DES),which are RANS near a wall and LES in the outer region, on the prolate spheroid for $\alpha < 30^o$. Like the URANS and LES mentioned above, an isotropic eddy viscosity model is used. Mean velocity profiles and separation location for the prolate spheroid are modeled fairly well. Perhaps what these URANS, LES, and DES results mean is that some of the anisotropy of a real flow can be simulated by the large scale unsteady motions.

SOME MODELING CONSIDERATIONS

It appears clear that the isotropic eddy viscosity approach to 3DTBL RANS modeling does not entirely capture the flow physics. As a result of the limitations of algebraic models to mimic the observed lags within these flows, a Reynolds-stress transport equation model is suggested with the normal-to-wall rms velocity fluctuation v' as the velocity scale, since it reflects the active shear stress-producing motions, and is contained in a turbulent stress production term. Clearly, this model cannot mimic the nature of the low-frequency vortices, which require LES, DES, or URANS.

Algebraic relations among some of the parameters in the transport equations have been revealed from the data base of 3-D experiments examined by Ciochetto and Simpson and summarized by Simpson et al. (1997). Eleven data sets, in addition to the ones examined by Ölçmen and Simpson (1995a), that encompass several different test geometries were examined: plane of symmetry flows with spanwise rates-of-strain; a 30^o bend flow; wing/body junction flow; pressure-driven flows with wall curvature; leeside flows on axisymmetric bodies at angles of attack; and shear-driven flows.

In these data sets and the Compton and Eaton (1997)flow with relatively mild 3-D effects, the $1/S=|\tau/\rho|/v'^2$ parameter correlates fairly well from station to station within a flow and between experiments, as long as embedded mean flow vortices are not present. The ratio 1/S approximates a constant for $0.3\text{-}0.4 < y/\delta < 0.7\text{-}0.8$ ranging from values of 0.5-0.8 with an overall average of approximately 0.7. At $y/\delta=1.0$, 1/S appears to have a mean value of approximately 0.3 for those sets. The parameter appears to be mildly affected by different 3D effects, however the effects were of the order of the uncertainties in the experiments. Ciochetto and Simpson also found that some algebraic parameters describing the turbulent triple products correlated data from many flows were less sensitive to three-dimensional effects than 1/S. As discussed by Simpson et al. (1997), the $v^3/[(uv^2)^2 + (v^2w)^2]^{1/2}$ and $v^3/(u^2v + v^3 + w^2v)$ are invariant to rotation about the y axis and relate the turbulent transport of the instantaneous stresses in the y direction. (The recent experiments of Kuhl and Simpson (2000) reveal the turbulence structure downstream of dual half-wing vortex generators and may be useful for examining streamwise vortices that begin from fixed locations.)

Recently compressor blade tip gap flows were examined by Tang and Simpson (2004) and Tian et al. (2004). Figure 10 shows the wall shear stress directions from surface oil flows for tip gap to chord ratio t/c = 3.3%. Under the blade the mean flow direction can vary almost 90^o. Figure 11 shows $1/S=|\tau/\rho|/v'^2$ vs. y^+ profiles. The "uu" far upstream profile is close to that for a 2-D flow. Note the much lower values of 1/S as one moves downstream on the suction side, indicating a much lower correlation between the shearing stresses and v'. No correlation between this reduction in/1/S and the difference between the flow direction and the shearing stress direction was found. These data show that extremely skewed flows produce a much different 1/S behavior than mildly skewed cases.

The viscous dissipation, the pressure diffusion, pressure/rate-of-strain, and turbulent diffusion terms in the transport equations also need to be modeled. Ölçmen and Simpson (1996b,c; 1997a) examined several second-order closure models in light of their detailed experimental data (Ölçmen and Simpson, 1997b) obtained for a 2DTBL and several locations shown in Figure 1 for the wing/body junction wind tunnel flow. Enough spatial data were obtained to determine the convective terms from data and perform a term-by-term examination of the Reynolds-stress transport equation budgets (Ölçmen and Simpson, 1996b). All terms except the dissipation rate (ϵ), pressure diffusion, and pressure/rate-of-strain (PRS) terms were evaluated directly using data. Using the TKE transport equation, the dissipation rate ϵ was estimated from the difference among other terms. An anisotropic dissipation distribution was used and produced stress transport equation budgets that were in better agreement with low Reynolds number direct numerical simulation (DNS) budgets than the isotropic dissipation case. The resulting pressure/rate-of-strain (PRS) terms for each transport equation and flow location were then compared by Ölçmen and Simpson (1996b,c) with 7 models. There is still a need for improved PRS models for 3D flows, especially near the wall in the -vw shearing stress transport equation.

Ölçmen and Simpson (1997a) used several turbulentdiffusion models to compare with the experimentally measured profiles. All models that were tested failed to capture the magnitude of the triple products, apparently due to the scaling factor q^2/ϵ. Note that since the experimentally measured turbulent diffusion terms were used in the transport equation budgets, Ölçmen and Simpson's conclusions about the PRS models do not depend upon a turbulent diffusion model.

The low Reynolds number channel flow DNS of Coleman et al. (2000) is particularly enlightening. Flows subject to impulsive

mean three-dimensionality with and without the mean deceleration of an adverse pressure gradient (APG) were considered. Strains simulating swept-wing and pure skewing (sideways turning) three-dimensional boundary layers were imposed. The APG influences the structure of the turbulence, measured for example by the ratio of shear stress to kinetic energy, much more than does the pure skewing. For both deformations, the evolution of the Reynolds stress was strongly affected by changes to the velocity-pressure-gradient correlation (VPGC) tensor. This term - which represents the finite time required for the mean strain rate to modify the shape and orientation of the turbulent motions - is primarily responsible for the difference (lag) in direction between the mean shear and the turbulent shear stresses, a well-known feature of perturbed three-dimensional boundary layers.

NEEDED FUTURE WORK

The 3DTBL and separated flows show some decorrelation between the generated shear stresses and TKE. Because of the non-equilibrium nature these flows and the anisotropy of the eddy viscosity, it is necessary to use Reynolds-averaged transport equations which can mimic the lags between the mean flow and the shearing stress structure. Work discussed here show that v' is closely related to the shear stress magnitude and triple products in a variety of non-equilibrium 3D experiments over a range of Reynolds numbers. Relationships for the pressure diffusion, pressure/rate-of-strain (PRS), turbulent diffusion, and dissipation rate are needed. The work quoted here shows that several uncertainties exist in the modeling of these terms, especially in the near-wall region. The relationships among pressure and velocity fluctuations remains an important modeling issue. LES, URANS, or DES are necessary to capture the low frequency motions that often accompany separation and with sufficient grid may capture enough of the anisotropy to permit isotropic subgrid modeling.

Experimental data are needed at high Reynolds numbers ($Re_\theta > 10^5$) for both attached and separated 3D flows to better determine the effect of Reynolds number on the flow structure. Data are needed for the velocity/pressure gradient correlation (VPGC) tensor in order to verify existing models and to develop better models, especially since these terms seem to account for the lag between the mean flow and the shearing stresses. New laser-Doppler velocimetry technologies can measure the acceleration/velocity correlation and the dissipation rate for high Reynolds numbers and obtain the VPGC by difference. See Lowe and Simpson (2005).

ACKNOWLEDGMENTS

The referenced 3DTBL work at VPI&SU has been supported by the Office of Naval Research, Drs. L.P. Purtell, E. Rood, R. Joslin, and Ki-Han Kim, Program Managers. K. Granlund, D. Hunter, and N. Varano contributed to the literature search and review for this paper.

REFERENCES

Alin, N., Fureby, C., Svennberg, S., Wikström, N., Sandberg, W., Ramamurti, R., Bensow, R., Persson, T., 2005, "3-D Unsteady Computations for Submarine-Like Bodies," AIAA-05-1044, *43rd Aero. Sci. Meeting*.

Bruns, J. M., Fernholz, H. H., and Monkewitz, P. A., 1999, "An experimental investigation of a three-dimensional turbulent boundary layer in an `S'-shaped duct," *J. Fluid Mech.* 393, 175-213.

Byun, G, and Simpson, R. L., 2005, "Structure of Three-Dimensional Separated Flow on an Axisymmetric Bump," AIAA-05-0113, *AIAA 43th Aero. Sci. Meeting*, 10-13 Jan.

Byun, G., Ölçmen, S. M., and Simpson, R. L., 2004, "A Three-velocity-component Sub-miniature LDV Turbulent Boundary Layer Measurements," *Meas. Sci. & Tech.*, vol. 15, pp. 2075-2082.

Byun, G., Simpson, R.L. and Long, C.H., 2003, "A Study of Vortical Separation from Three-dimensional Symmetric Bumps,"AIAA-2003-0641; *AIAA J.*, 42, no. 4, 754 - 765, 2004.

Chesnakas, C.J. and Simpson, R.L. ,1997, "Detailed Investigation of the Three-Dimensional Separation About a 6:1 Prolate Spheroid," *AIAA J.*, Vol. 35, no. 6, pp. 990 - 999.

Coleman, G. N., Kim, J. and Spalart, P. R., 2000, "A Numerical Study of Strained Three-dimensional Wall-bounded Turbulence," *J. Fluid Mech.*, vol. 416, pp.75-116.

Compton, D. A. and Eaton, J. K., 1997, "Near-Wall Measurements in a Three-Dimensional Turbulent Boundary Layer," *J Fluid Mech.*, vol. 350, pp.189-208.

Cummings, R., Forsythe, J., Morton, S., Squires, K., 2003, "Computational Challenges in High Angle of Attack Flow Prediction," *Prog. Aero. Sci.*, vol.39, no.5, pp.369-384.

Davidson, L. and Dahlström, S., 2005, "Hybrid LES-RANS : Computation of the Flow around a Three-Dimensional Hill", *Int. Symp. Eng. Turb. Modelling and Measurements*, Italy, May.

Deng, G. and Visonneau, M., 1999, "Computation of a Wing-body Junction Flow with a New Reynolds-stress Transport Model," *Proc. 22nd Symp. Naval Hydro.*, pp. 691-707, Natl. Acad Press.

Eaton, John K., 1995, "Effects of Mean Flow Three Dimensionality on Turbulent Boundary-Layer Structure," *AIAA J.* Vol. 33, pp. 2020-2025.

Fleming, J.L. and Simpson, R.L.,1997, "Experimental Investigation of the Near Wall Flow Structure of a Low Reynolds Number 3-D Turbulent Boundary Layer," VPI-AOE-247; DTIC.

Fureby, C., Alin, N., Wikström, N., Menon, S., Svanstedt, N. and Perrson, L., 2004, "Large-Eddy Simulation of High-Reynolds-Number Wall-Bounded Flows", *AIAA J.*, vol. 42, pp. 457-468.

George, J. and Simpson, R.L. 2002 "Some Three-dimensional Rough-wall Turbulent Boundary Layers," AIAA-2002-0580, *40th AIAA Aerospace Sci. Meeting*, Jan. 14-17.

George, J. And Simpson, R.L., 2005, "Structure of 2-D and 3-D Turbulent Boundary Layers with Sparsely Distributed Roughness Elements," VPI-AOE-292; DTIC.

Goody, M.C. and Simpson, R.L.,1999,"An Experimental Investigation of Surface Pressure Fluctuations Beneath 2-D and 3-D Turbulent Boundary Layers," AIAA-99-0608; also *AIAA J.*, vol. 38, pp. 1822 - 1831, 2000.

Goody, M. C., Simpson, R. L. and Chesnakas, C. J., 1997, "Separated Flow Surface Pressure Fluctuations and Pressure-Velocity Correlations on Prolate Spheroid," AIAA-97-0485; also *AIAA J.*, vol. 38, no. 2, pp. 266 - 274, 2000.

Goody, M., Simpson, R.L., Engel, M., Chesnakas, C. and Devenport, W., 1998, "Mean Velocity and Pressure and Velocity Spectral Measurements within a Separated Flow Around a Prolate Spheroid at Incidence," AIAA-98-0630, *36th AIAA Aero. Sci.*

Ha, S. and Simpson, R.L., 1993, "An Experimental Investigation of a Three-dimensional Turbulent Boundary Layer Using Multiple-sensor Probes," *Ninth Symp. Turbulent Shear Flows*, Kyoto, Japan, 16-18 Aug. , p. 2-3-(1 - 6); VPI-AOE-205, 1993, DTIC.

Johnston, J. P. and Flack, K. A., 1996, "Review - Advances in Three-Dimensional Turbulent Boundary Layers with Emphasis on the Wall-Layer Regions," *J. Fluids Eng.*, vol. 118, pp. 219 - 232.

Jongen, T., Mompean, G. and Gatski, T. B., 1998, "Predicting S-Duct Flow Using a Composite Algebraic Stress Model," *AIAA J.* Vol. 36, pp. 327-335.

Kotapati-Apparao, R., Squires, K., Forsythe, J.,2003, "Prediction of a Prolate Spheroid Undergoing a Pitchup Maneuver," AIAA-03-0269, *AIAA 41st Aero. Sci.* Meeting, Reno, NV.

Kuhl, D.D. and Simpson, R.L., 2000, "Near-wall Investigation of a Stream-wise Vortex Pair," paper 27.1, *10th Inter. Symp. Appl. Laser Techniques to Fluid Mech.*, July 10-13, Lisbon, Portugal; also VPI-AOE-273, 2001; DTIC.

Lowe, K. T. and Simpson, R.L., 2005, "Measurements of Velocity-acceleration Statistics in Turbulent Boundary Layers," in current TSFP-4 volume.

Ma, Ruolong and Simpson, R.L., 2005, "Characterization of Turbulent Flow Downstream of a Three-dimensional Axisymmetric Bump," in current TSFP-4 volume.

Madden, M.M. and Simpson, R.L., 1997, "Octant Analysis of the Reynolds Stresses in the Three-dimensional Turbulent Boundary Layer of a Prolate Spheroid," VPI-AOE-252;DTIC.

Morrison, J., Panaras, A., Gatski, T., Georgantopoulos, G., 2003, "Analysis of Extensive Cross-Flow Separation using Higher-Order RANS Closure Models," AIAA-03-3532, *AIAA 21st Applied Aero. Conf*, Orlando, FL.

Ölçmen, S.M. and Simpson, R.L., 1995a, "An Experimental Study of Three-dimensional Pressure-Driven Turbulent Boundary Layer," *J.Fluid Mech.*, Vol. 290, pp. 225 - 262.

Ölçmen, S.M. and Simpson, R.L., 1995b, "A 5-Velocity-Component Laser-Doppler Velocimeter for Measurements of a Three-Dimensional Turbulent Boundary Layer," *Meas. Sci. & Tech.*, Vol. 6, pp. 702 - 716.

Ölçmen, S. M., and Simpson, R.L., 1996a, "An Experimental Study of a Three-Dimensional Pressure-Driven Turbulent Boundary Layer: Data Bank Contribution," *J. Fluids Eng.*, vol. 118, pp. 416 - 418.

Ölçmen, S. M., and Simpson, R.L., 1996b, "Experimental Transport-rate Budgets in Complex Three-dimensional Turbulent Flows at a Wing/Body Junction," *27th AIAA Fluid Dynamics Conf.*, AIAA-96-2035, New Orleans, June 17-20.

Ölçmen, S. M., and Simpson, R.L., 1996c, "Theoretical and Experimental Pressure-strain Comparison in a Pressure-driven Three-dimensional Turbulent Boundary Layer," *1st AIAA Theor. Fluid Mech. Meeting*, AIAA-96-2141, New Orleans, June 17-20.

Ölçmen, S.M. and Simpson, R.L., 1997a, "Experimental Evaluation of Turbulent Diffusion Models in Complex 3-D Flow Near a Wing/Body Junction," AIAA-97-650, *35th AIAA Aero. Sci. Meeting*, Jan. 6 - 10.

Ölçmen, S.M. and Simpson, R.L., 1997b, "Some Features of a Turbulent Wing-Body Junction Vortical Flow," AIAA-97-0651, *35th AIAA Aero. Sci. Meeting*; VPI-AOE-238; DTIC, 1996.

Ölçmen, S.M., George, J., and Simpson, R.L., 1999, "Experimental Study of High Reynolds Number (Re_θ = 23000) Two and Three-dimensional Turbulent Boundary Layers," AIAA-99-0553 & AIAA-99-0554, *37th AIAA Aero. Sci. Meeting*, Jan. 11-14; *Exp. Fluids*, vol. 31, pp. 219 - 228, 2001.

Ölçmen, S. M., Simpson, R.L., and Goody, M.C., 1998, "An Experimental Investigation of Two-Point Correlations in Two- and Three-Dimensional Turbulent Boundary Layers," AIAA-98-0427; *Flow, Turb. and Combustion*, Vol. 66, pp.85-112, 2001.

Ölçmen, S. M., Simpson, R.L., and Newby, J., 2005, "Octant Analysis Based Structural Relations for Three-dimensional Turbulent Boundary Layers," in current TSFP-4 volume.

Paik, J., Ge, L. and Sotiropoulos, F., 2004, "Toward the Simulation of Complex 3D Shear Flows using Unsteady Statistical Turbulence Models, *Int. J. Heat & Fluid Flow*, vol. 25, pp.513-527.

Patel, N., Stone, C. and Menon, S., 2003, "Large-Eddy Simulation of Turbulent Flow Over an Axisymmetric Hill," AIAA-2003-0967, *41st AIAA Aero. Sci. Meeting.*

Rhee, S. and Hino, T., 2002, "Numerical Simulation of Unsteady Turbulent Flow Around Maneuvering Prolate Spheroid," *AIAA J.*, vol. 40, pp. 2017-2026.

Rizzi, A. and Vos, J., 1998, "Towards Establishing Credibility in Computational Fluid Dynamics Simulations," *AIAA J.*, vol. 36, pp. 668 - 675.

Simpson, R. L., 1996, "Aspects of Turbulent Boundary Layer Separation," *Prog. Aerospace Sci.*, Vol. 32, pp. 457 - 521.

Simpson, R. L., 2001, "Juncture Flows," *Annual Review of Fluid Mechanics*, Vol. 33, pp. 415 - 441.

Simpson, R.L., Long, C.H. and Byun, G., 2002, "Study of Vortical Separation from an Axisymmetric hill," *Int. J. Heat & Fluid Flow,* vol. 23, pp. 582-591.

Simpson, R.L., Ölçmen, S.M., Fleming, J.L., and Ciochetto, D. S., 1997, "Some Structural Features of Pressure-driven Three-dimensional Turbulent Boundary Layers From Experiments," *ICASE/LaRC/AFOSR Symp. Modeling Complex Turbulent Flows*, Aug., 11-13, 1997; in *Modeling Complex Turbulent Flows*, M. Salas, J. Hefner, and L. Sakell, ed.; pp.223 - 243, Kluwer.

Sreenivas, K., Hyams, D., Nichols, S., Mitchell, B., Taylor, L., Briley, R., Whitfield, D., 2005, "Development of an Unstructured Parallel Flow Solver for Arbitrary Mach Numbers," AIAA -05-0325, *AIAA 43rd Aero. Sci. Meeting.*

Suga, K., 2003, "Predicting Turbulence and Heat Transfer in 3-D Curved Ducts by Near-wall Second Moment Closures, *Int. J. Heat & Fluid Flow*, vol. 46, pp. 161-173.

Tang, G. and Simpson, R.L., 2004, "Measurements of the Tip-Gap Turbulent Flow Structure in a Low-speed Compressor Cascade," Report VPI-AOE-288; DTIC.

Taylor, L., Pankajakshan, R., Briley, W., Whitfield, D., 2005, "Scalable Parallel Implicit Algorithm for Advanced Turbulence Closures," AIAA-05-0876, *AIAA 43rd Aero. Sci. Meeting.*

Temmerman, L., Wang, C. and Leschziner, M.A., 2004, "A Comparative Study of Separation from a Three-Dimensional Hill Using LES and Second-Moment-Closure RANS Modeling", *Euro. Cong. Comp. Methods in Applied Sci. & Eng.*, July.

Tian, Q., Simpson, R.L., and Tang, G., 2004, "Surface oil flow visualization in the linear compressor cascade," *Meas. Sci. Tech.*, vol. 15, pp. 1910-1916.

Wang, C., Jang, Y.J. and Leschziner, M.A., 2004, "Modelling Two- and Three-Dimensional Separation from Curved Surfaces with Anisotropy-Resolving Turbulence Closures," *Int. J. Heat & Fluid Flow*, vol. 25, 499-512.

Webster, D. R., DeGraaff, D. B., and Eaton, J. K., 1996, "Turbulence Characteristics of a Boundary Layer Over a Swept Bump," J. Fluid Mech., vol. 323, pp. 1-22.

Wetzel, T.G. and Simpson, R.L., 1998, "Unsteady Three-dimensional Crossflow Separation Location Measurements on a 6:1 Prolate Spheroid Undergoing Time-dependent Maneuvers," *AIAA J.*, vol. 36, pp. 2063-2071.

Wetzel, T.G., Simpson, R.L., and Chesnakas, C.J., 1998, "The Measurement of 3-D Crossflow Separation," *AIAA J.*, vol. 36, pp. 557 - 564.

Wu, X. and Squires, K. D., 1998, "Prediction of the 3-D Turbulent Boundary Layer over a Swept Bump," *AIAA J*, 36, pp. 505-514.

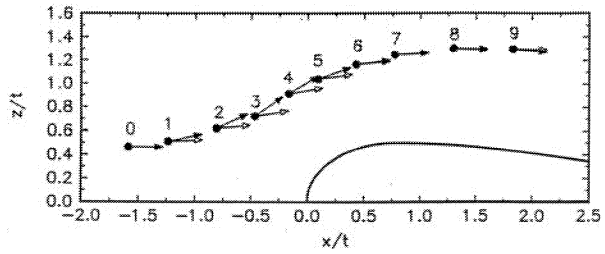

Figure 1. Top view of half wing shape and measurement locations. Full arrows – wall shear stress direction; open arrows – local free-stream direction. (Ölçmen et al., 1999)

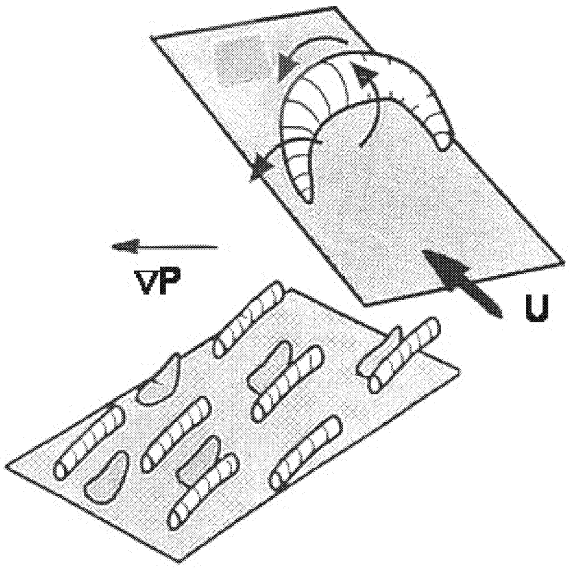

Figure 2. Coherent structures in a skewed 3DTBL. Outer "croissant-shaped" structures that entrain free-stream fluid move in different directions than near wall stream-wise vortical structures.

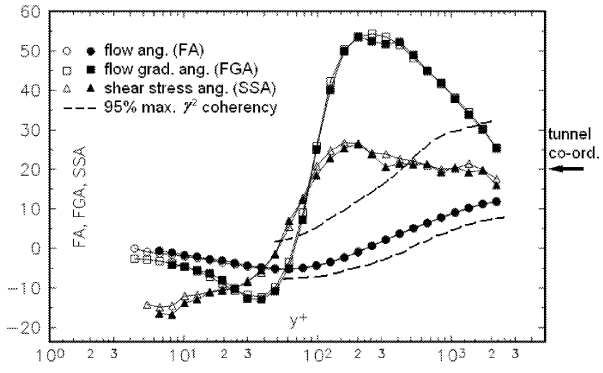

Figure 3. Station 5 flow angle [FA = arctan(W/U)], flow gradient angle [FGA= arctan(∂W/∂y)/(∂U/∂y)], shear stress angle [SSA= $\arctan(-\overline{vw}/-\overline{uv})$] calculated using two separate data sets in wall stress direction co-ordinates ((Ölçmen & Simpson, 1995a, 1997b). Coherency bounds from Ha and Simpson (1993) data.

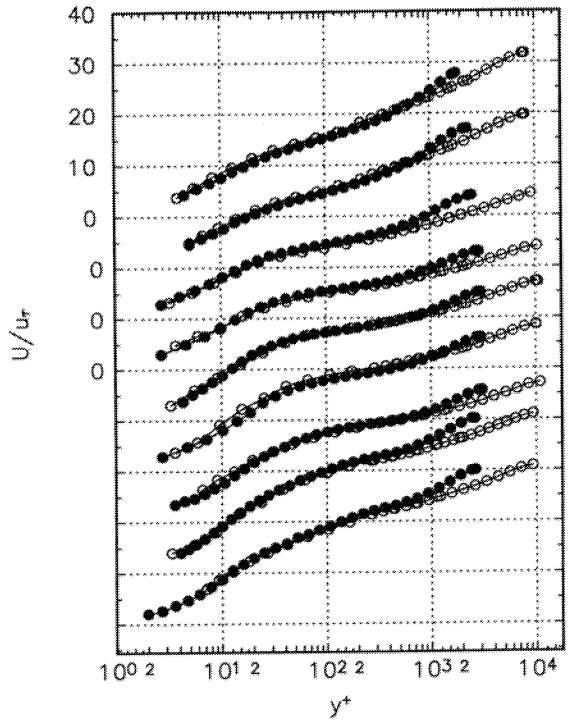

Figure 4. U^+ vs. y^+ mean velocity profiles in local wall shear stress co-ordinates. Solid, approach $Re_\theta = 5940$; open, $Re_\theta = 23{,}200$. (Ölçmen et al., 1999)

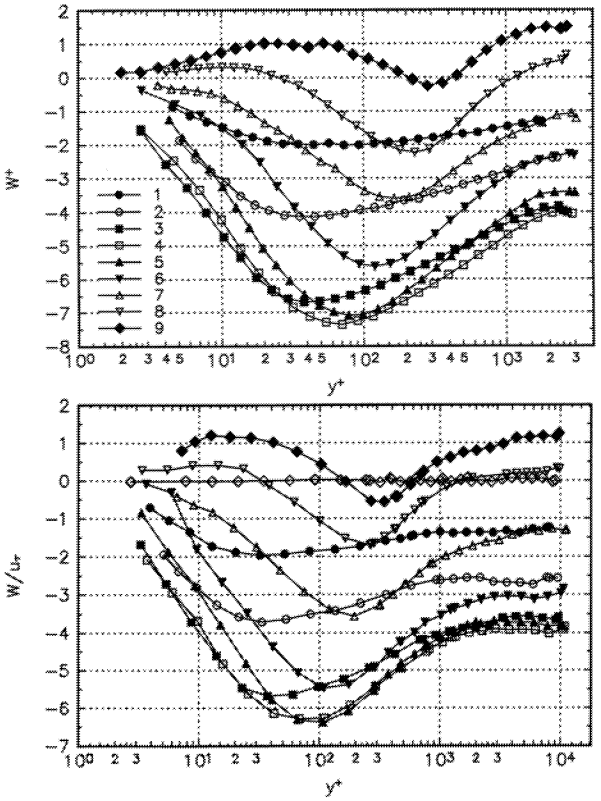

Figure 5. W/U_τ in tunnel co-ordinates with same legend. Top, approach $Re_\theta = 5940$; bottom, $Re_\theta = 23{,}200$.

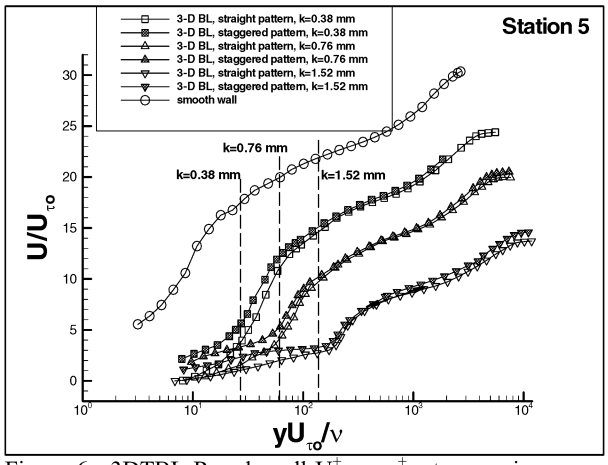

Figure 6. 3DTBL Rough wall U^+ vs. y^+ stream-wise mean velocity profiles at Station 5 in tunnel co-ord. (TC). (George and Simpson, 2002)

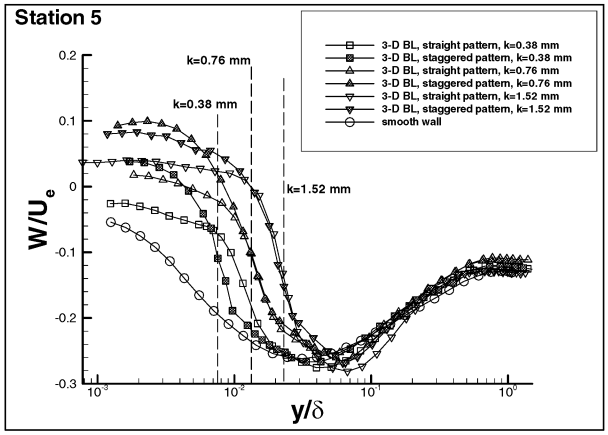

Figure 7. 3DTBL rough wall W/U_e vs. y/δ mean velocity profiles in TC for Station 5. (George and Simpson, 2002)

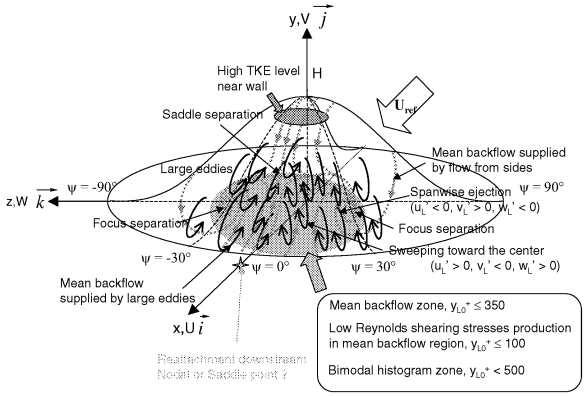

Figure 8. Illustration of flow structures on leeside of bump. Large eddies shown in black; near surface flow patterns in dashed; mean backflow zone in gray. (Byun and Simpson, 2005)

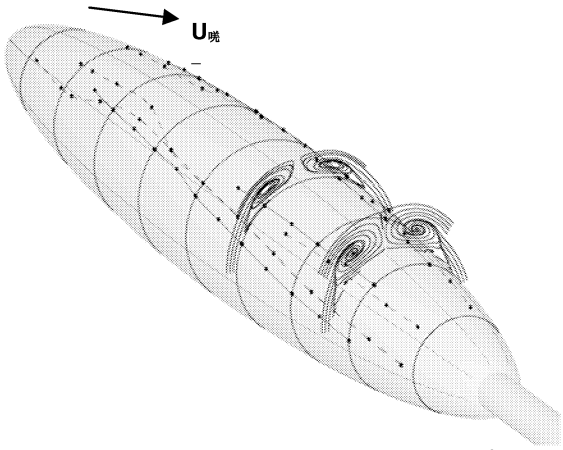

Figure 9. Flowfield for 6:1 prolate spheroid at $\alpha = 20^o$. Solid lines are oilflow separation line. Dashed lines show local minima in skin friction. (Wetzel et al., 1998).

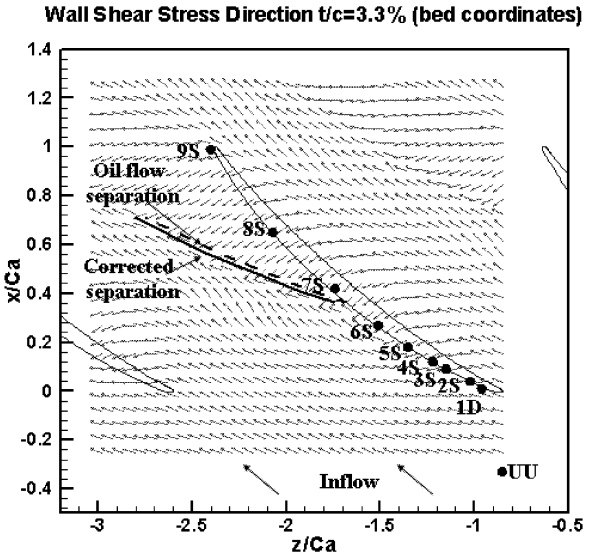

Figure 10. Compressor blade endwall flow directions and data locations for Fig. 11. (Tian, et al., 2004)

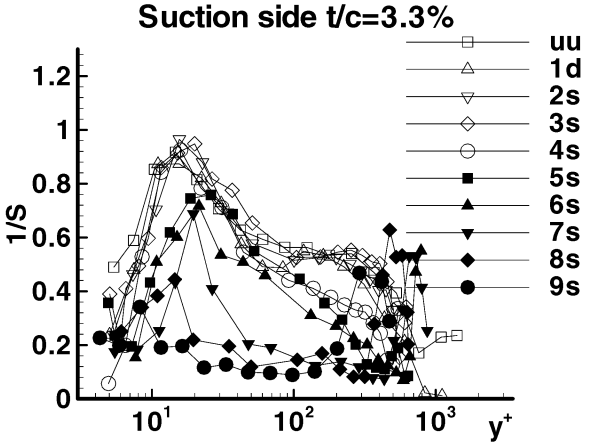

Figure 11. 1/S vs y^+ from endwall along compressor blade suction side. (Tang and Simpson, 2004)